nature chemistry

REVIEW ARTICLE

PUBLISHED ONLINE: 22 MAY 2012 | DOI: 10.1038/NCHEM.1352

The gold–sulfur interface at the nanoscale

Hannu Häkkinen

Thiolate-protected gold surfaces and interfaces, relevant for self-assembled monolayers of organic molecules on gold, for passivated gold nanoclusters and for molecule–gold junctions, are archetypal systems in various fields of current nanoscience research, materials science, inorganic chemistry and surface science. Understanding this interface at the nanometre scale is essential for a wide range of potential applications for site-specific bioconjugate labelling and sensing, drug delivery and medical therapy, functionalization of gold surfaces for sensing, molecular recognition and molecular electronics, and gold nanoparticle catalysis. During the past five years, considerable experimental and theoretical advances have furthered our understanding of the molecular structure of the gold–sulfur interface in these systems. This Review discusses the recent progress from the viewpoint of theory and computations, with connections to relevant experiments.

The covalent bond between gold and sulfur gives rise to a robust but modifiable interaction that is of paramount importance in stabilizing nanostructures and transmitting electronic interactions between gold and sulfur-containing organic molecules[1–16]. These interactions, mediated usually through the sulfhydryl (SH) functional group in thiols (RSH), are used in a very wide range of studies in molecular biology, inorganic chemistry, surface science and materials science, with potential applications in site-specific bioconjugate labelling and sensing[17,18], drug delivery and medical therapy[19–21], functionalization of gold surfaces for sensing, molecular recognition and molecular electronics[22], gold nanoparticle catalysis, and linking individual biomolecules and other organic molecules to gold. In these fields, self-assembled monolayers (SAMs) of thiols on planar gold surfaces, thiol-stabilized gold nanoclusters and thiol-stabilized molecular junctions between gold electrodes are archetypal systems that have been studied for decades. Given the ubiquitous use of the gold–sulfur interface, it is surprising that, until recently, detailed information on the atomic structure of that interface has largely been missing.

It is currently widely accepted that the covalent interaction at the gold–sulfur interface requires formation of gold–thiolate bond(s): that is, the sulfhydryl group is deprotonated, creating formally a thiyl radical ($RS^{\bullet}$), whereas the protonated SH group can interact with gold only by weaker coordination-type bonds through the sulfur lone-pair electrons. The thiolate–gold (RS–Au) bond has a strength close to that of the gold–gold bond, so it can significantly modify the gold–gold bonding at the gold–sulfur interface. The importance of this detail has become clear only in the past five years or so, when new experimental and theoretical evidence has become available about interfacial structures in thiolate-SAMs on Au(111), atomic structures of thiolate-protected gold nanoclusters and gold–thiolate–gold molecular junctions. The new information has been gathered through various techniques such as scanning tunnelling microscopy (STM), low-energy electron diffraction (LEED), surface-sensitive X-ray spectroscopic techniques such as grazing-incidence X-ray diffraction (GIXRD) and normal incidence X-ray standing waves (NIXSW), photoemission core-level spectroscopy, total structure determination via single-crystal X-ray crystallography, and density-functional theory (DFT) computations.

Many reviews have appeared in the fields of thiolate-SAMs on noble metal surfaces[1–7], thiolate-protected metal (mostly gold) nanoparticles[8–12] and molecular junctions[13–16]. This Review focuses on gold–thiolate systems and discusses the developments during the past five years or so that have led to the present understanding of the common structural features (schematically[23] shown in Fig. 1) that are present at the gold–sulfur nano-interface, and the consequent implications for the chemical protection (passivation), electronic structure and electrical conductance through that interface. Although the viewpoint is largely that of theory and computations, relevant experiments are discussed as well. In fact, the interplay between experiment and theory has greatly aided in developing the current understanding of the gold–sulfur nano-interface.

Gold–thiolate bonding in molecular complexes

Although gold is inert and chemically very 'uninteresting' in bulk form, it has rich ligand chemistry in nanometre-scale molecular complexes[24–26]. This is partially due to the existence of several possible oxidation states of gold when it is bound to ligands; oxidation states from –I to +V are known. Various complexes containing thiolates are interesting for biological and medical applications, for chemical diagnostics and even for the mining industry[27–32].

From the coordination chemistry viewpoint, gold is most often found in oxidation states of +I (linear ligand–Au(I)–ligand binding) and +III (square-planar binding to four ligands). Relativistic effects are important for understanding the electronic structure of a single gold atom, and these effects transmit to binding interactions with other gold atoms or with ligand molecules[25,33]. Generally, the relativistic effects induce contraction of the *s* and *p* shells in a given atom, which leads to a slight expansion of *d* and *f* shells due to increased electrostatic screening of the positive nucleus by the *s* and *p* electrons. Systematic analysis of the elements in the two lowermost rows of the Periodic Table has shown that the relativistic contraction of the 6*s* shell has a pronounced maximum at $Z = 79$ corresponding to gold[34]. Three important consequences follow. (i) The 'size' of the neutral gold atom is close to that of silver, and the ionic radius of the oxidized Au(I) (62 pm) is even smaller than that of Ag(I) (68 pm). (ii) The relativistic effects also shrink the energy separation between 5*d* and 6*s* shells of gold (5*d* split to $5d_{3/2}$, $5d_{5/2}$ subshells) enabling easy *sd* hybridization on bonding to neighbouring atoms. (iii) Aurophilic effects (weak $5d^{10}$–$5d^{10}$ attraction)

Departments of Physics and Chemistry, Nanoscience Center, University of Jyväskylä, FI-40014 Jyväskylä, Finland.
e-mail: Hannu.J.Hakkinen@jyu.fi

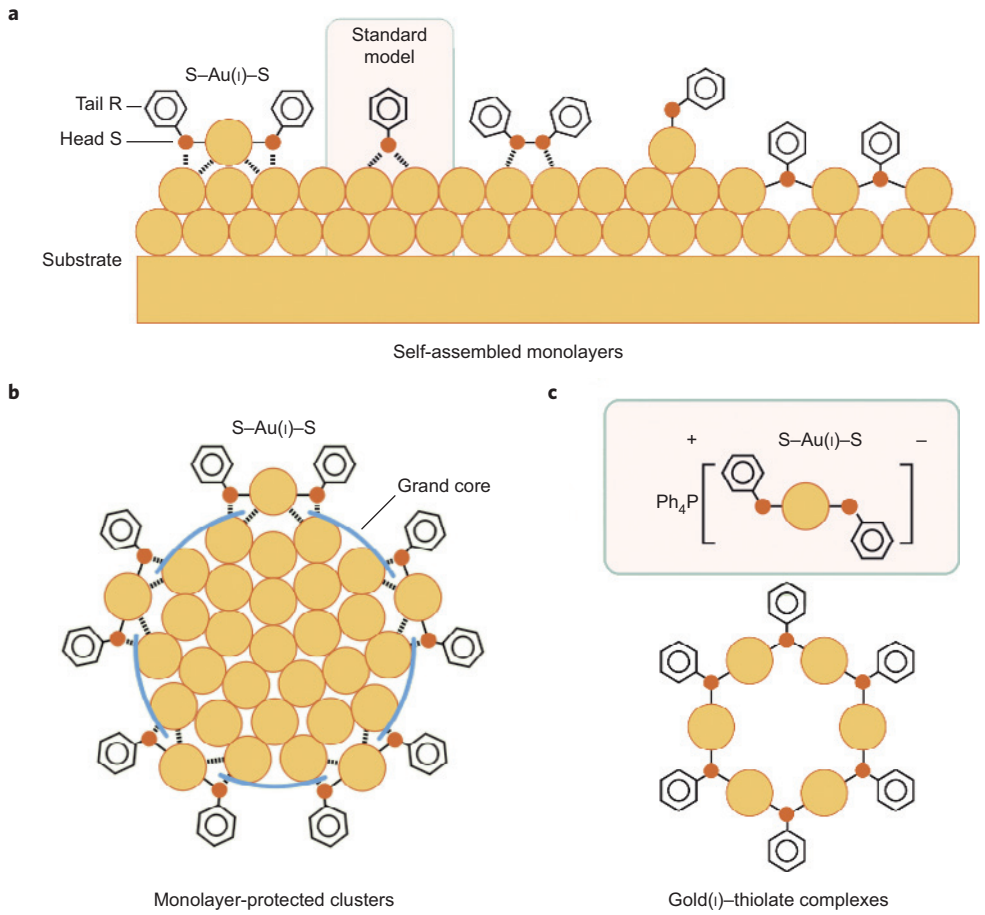

Figure 1 | Schematics of bonding motifs between thiolates and gold. a, Over the past 20 years, several atomic structures for the gold–sulfur interface of the close-packed thiolate-SAM on Au(111) have been suggested. The 'standard model' describing a monothiolate binding at atop, bridge or hollow site on an unreconstructed Au(111) surface has been challenged by (from middle to right): disulfide bonding, a complex involving an Au adatom and a thiolate (Au–SR), and a polymeric chain structure where monothiolates are bridging Au adatoms. New experimental and theoretical evidence shows that a key structural unit in the low- and medium-coverage SAM layer may be the complex RS–Au(I)–SR where the bridging gold atom is in a formal oxidation state of +1 (left). **b**, This structural unit has recently been observed also at the gold–thiolate interface of thiolate-protected gold nanoclusters from X-ray single crystal studies. **c**, Polymeric ring-like $(RSAu)_n$ or chain-like $RS(AuSR)_n$ Au(I)-thiolate compounds have been structurally characterized as well. Figure adapted with permission from ref. 23, © 2007 AAAS.

become important for complexes that contain several Au(I) centres, and this interaction may contribute to the internal structure.

In recent years, a number of DFT computations of gold(I)–thiolate complexes have appeared, and some of these studies include comparison to other noble metal(I)–thiolate complexes[35–40]. Systematic comparison of the metal–thiolate bond for noble metal monothiolates[38] has shown that although all the noble metal–SR bonds show a degree of covalency, the Cu–SR bond is most polarized and the Au–SR bond is least polarized, shown by, for example, charge analysis by the Bader method[41] (Fig. 2a). Similar charge reorganization is observed for stoichiometric $(AuSR)_n$ complexes, which can be ring-like (Fig. 2c), crown-like or helical. Conceptually, it is useful to consider sp^3-type hybridization in the sulfur, with two of the four S(sp^3) hybrid orbitals making covalent bonds to the Au(6*s*) electrons at a roughly 90° angle. In reality, the gold–sulfur bond also includes important contributions from Au(*d*) electrons[35]. Many structural and electronic properties of the stoichiometric $(AuSR)_n$ complexes, such as Au–S bond length, bonding angles S–Au–S and Au–S–Au, addition energy of one AuSR unit to the complex, and the molecular HOMO–LUMO energy gaps, converge at about $n = 4$ (refs 35,39). The nature of the thiolate ligand can affect the geometry slightly through steric effects, and the degree of electron affinity of the organic part may also change the HOMO–LUMO and optical gaps (Fig. 2d).

Non-stoichiometric $RS(AuSR)_n$ ($n = 1, 2\ldots$) complexes (Fig. 2b) are relevant for the later discussion in this Review on thiolate-protected flat and curved gold surfaces (SAM/Au(111) and thiolate-protected gold clusters, respectively). In the neutral state these complexes are odd-valence-electron systems (radicals). The LUMO state (HOMO of the corresponding anion) has a configuration with notable sulfur *p*-character and weak gold *d*-character (Fig. 2b). The Au–S bond expands slightly (from 2.27 Å to 2.32 Å) on adding the electron to the neutral complex, indicating that the LUMO of the neutral complex has an antibonding Au–S character. Intracomplex Au–S distances of 2.32–2.35 Å are typically calculated for $RS(AuSR)_n$ ($n = 1,\ 2$) units on Au(111) surfaces and at the surface of thiolate-protected gold nanoclusters; this indicates that these complexes localize one additional electron, becoming formally anionic in those situations. Recently, anionic $CH_3S(AuSCH_3)_n^-$ ($n = 1, 2$) complexes were successfully characterized in the gas phase by means of photoelectron spectroscopy[40]. The measured vertical detachment energies for the anions are high, about 3.5 eV ($n = 1$) and 4.1 eV ($n = 2$). The photodetachment peaks are sharp at temperature $T = 20$ K, but become broad at room temperature, which was ascribed to the many conformations of the methyl groups on the basis of accompanying density functional theory (DFT) calculations.

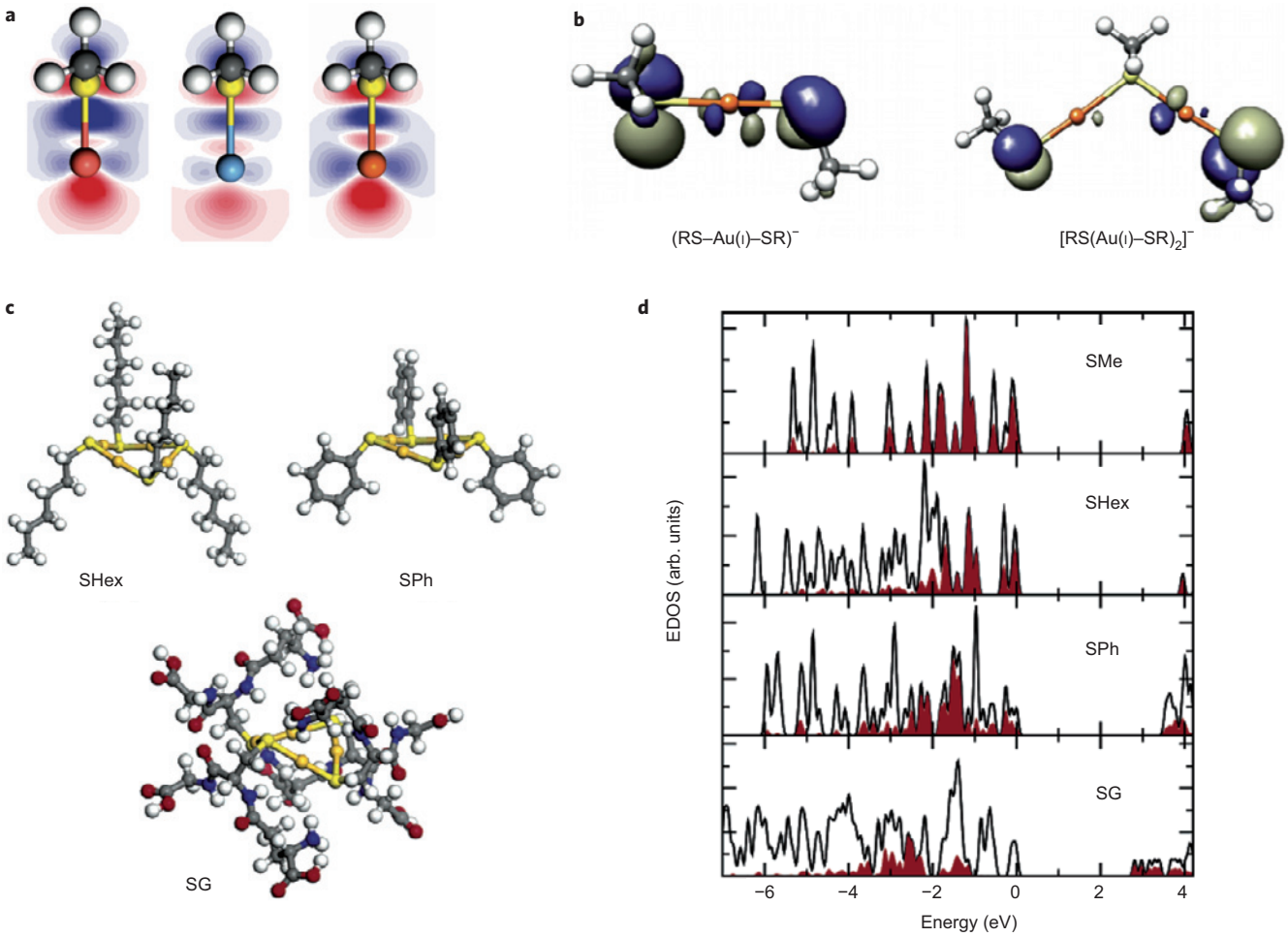

Figure 2 | Computed structures, bonding motifs and electronic states of gold–thiolate complexes. a, Reorganization of electron charge on formation of the metal–sulfur bond in noble metal monothiolates: $CuSCH_3$ (left), $AgSCH_3$ (middle) and $AuSCH_3$. The contours are plotted in a plane containing the metal and the sulfur. Blue and red correspond to respective accumulation and depletion of electron charge on bond formation. Bader charge analysis shows a slight positive charging of metal atoms (Cu +0.34 |e|; Ag +0.27 |e|; Au +0.09 |e|). **b**, Visualization of the HOMO of anionic complexes $(RSAuSR)^-$ and $[RS(AuSR)_2]^-$ with R = methyl. The orbital symmetries correspond to *p* orbitals at the terminating sulfurs. **c**, DFT-optimized structures of $Au_4(SR)_4$ ring with hexylthiolates (SHex), benzenethiolates (SPh) and glutathionates (SG). **d**, Electronic density of states (EDOS) for $(AuSR)_4$ complexes with methylthiolates (SMe), hexylthiolates, phenylthiolates and glutathionates. The shaded area corresponds to projection to Au orbitals. The energy of the HOMO state is at zero. Parts **a** and **b** reproduced with permission from ref. 38, © 2010 ACS; parts **c** and **d** reproduced with permission from ref. 35, © 2006 ACS.

Thiolate–Au(111) self-assembled monolayers

Gold surfaces offer a convenient substrate for SAM formation because they are easy to prepare and clean, owing to the chemical inertness of gold under ambient conditions. Thiolate-SAMs on gold surfaces (usually Au(100) or Au(111)) can be formed by using monothiols (RSH), thioethers (RSR) or disulfides (RSSR), where R is an alkyl or an aryl group. The first report on thiolate-SAMs on gold, back in 1983, dealt with solution-adsorbed organic disulfides[42], and the work soon expanded to other organosulfur–gold systems (for early reviews, see refs 1 and 2). This discussion focuses on the Au(111) surfaces.

For both alkyl and aryl thiolates, different phases corresponding to different ordering of the R-groups on Au(111) have been observed. For low-coverage adsorption, one frequently observes the 'striped' phase that, for longer alkylthiolates, shows a 'lying-down' configuration with the alkyl chains oriented approximately parallel to the surface. For ordered higher-coverage SAMs, a 'standing up' phase is observed where the R groups are packed vertically. Close-packing is influenced greatly by the weak but long-range dispersion forces and steric effects. In this phase the interfacial Au–S layer structure is particularly difficult to probe, owing to the inaccessibility of the interface to direct imaging and the need to use surface-sensitive spectroscopy, mainly variants of the X-ray standing wave (XSW), photodiffraction, helium diffraction or electron diffraction methods. It was suggested early on that the thiolates occupy three-fold hollow positions on an unreconstructed Au(111) surface and the geometry of the full monolayer is that of $(\sqrt{3} \times \sqrt{3}R30°)$[43]. Initial helium diffraction[44] and electron diffraction[45,46] studies supported this interpretation, but later helium diffraction experiments revealed a $c(4 \times 2)$ superstructure on top of the $(\sqrt{3} \times \sqrt{3}R30°)$ lattice. All these structures imply a 1/3 thiolate coverage for the full SAM monolayer, with respect to Au sites in an unreconstructed Au(111) layer.

The adsorption mode involving only monothiolates was questioned when the first XSW experiments were interpreted in terms of disulfide adsorption[47,48]. The first implication of the existence of Au–S bonds perpendicular to the interface came from photodiffraction and XSW experiments in 2003/04 indicating Au top-site adsorption of thiolates[49,50]. These results were initially interpreted in terms of AuSR complexes that may be very mobile on non-defected

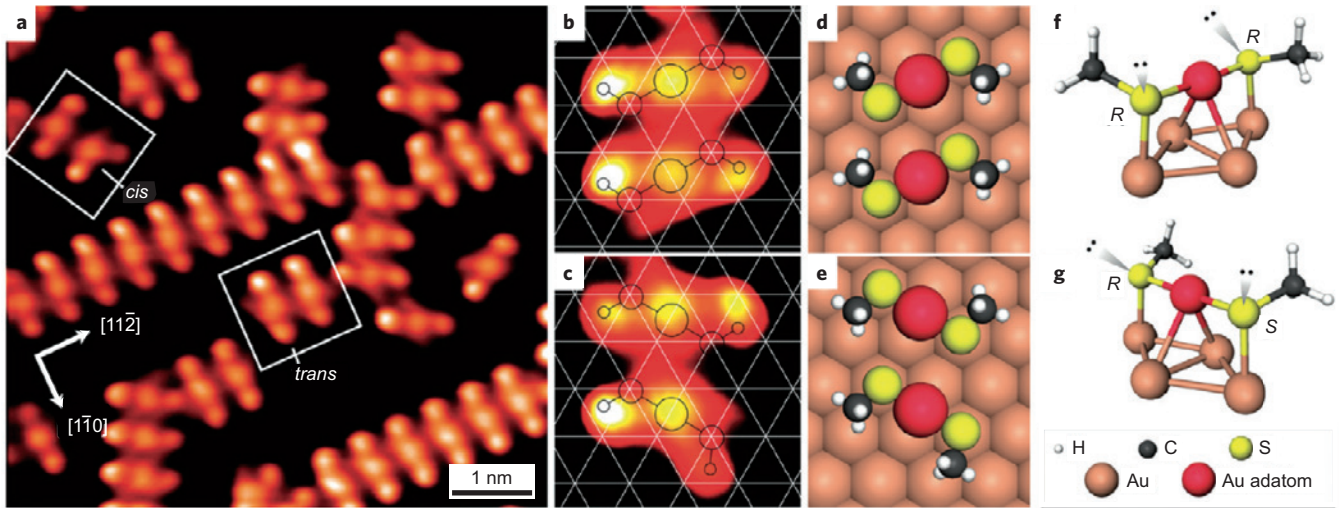

Figure 3 | STM images and atomistic interpretation of the structure of the low-coverage striped phase of methylthiolates CH_3S on Au(111). a, The self-assembled striped patterns are formed by heating a gold crystal pre-dosed with dimethyldisulfide above 200 K for about 10 min. **b**,**d**, Close-up image of a pair of *trans*-CH_3S–Au–SCH_3 complexes and its atomistic model. **c**,**e**, Corresponding image of a *cis*–*trans* pair. **f**,**g**, DFT-optimized structures of the (*R*,*R*)-*trans* (part **f**) and (*R*,*S*)-*cis* (part **g**) complexes. The *R*-configuration of the chiral sulfur centre is defined in the following order of the sp^3-type directions: the lone electron pair, CH_3, surface Au atom, Au atom in the complex. Figure reproduced with permission from ref. 55, © 2009 ACS.

Au(111) and could be the key structural component in the SAM formation, in line with a model suggested from DFT computations[51]. This requires the existence of easily available Au adatoms on Au(111) during SAM formation, which is consistent with observations of lifting of the 'herringbone' (22 × √3) reconstruction and formation of surface vacancy islands ('etch pits'). Together these processes can be estimated to release enough adatoms for the gold–thiolate complex formation.

STM evidence of RS–Au–SR complexes on Au(111) at low thiolate coverage. Recent STM studies on low-coverage striped phases of methyl- and phenylthiolates on Au(111)[52–55] have greatly changed the understanding of the atomic structure of the Au(111)/SR interface. These experiments have consistently shown formation of RS–Au–SR complexes (R = CH_3 or R = Ph) (Fig. 3). In these complexes, the central Au atom is linearly coordinated by surface-parallel bonds to the two thiolates, bridging two Au atoms underneath in the first surface layer, and the sulfurs adopt Au on-top sites. It is instructive to think the local electronic structure of the sulfur as being of sp^3 type where the electrons participate in four different kinds of interactions: with the R group, with the two non-equivalent Au atoms (Au in the complex and Au in the surface layer) and in a lone-pair orbital. This special bonding motif creates a chiral centre at the sulfur, so the thiolate ends of the RS–Au–SR complex can be classified as *R*- and *S*-enantiomers (Fig. 3f,g). Any single thiolate–gold–thiolate complex includes sulfur atoms of either the same type (*R*,*R* or *S*,*S*), creating a thiolate–gold–thiolate *trans*-isomer, or an (*R*,*S*) pair, creating a *cis*-isomer. DFT computations yield *cis*- and *trans*-complexes as thermodynamically almost equivalent, as the difference in the adsorption energy is only of the order of 0.1 eV. The calculated activation barrier for *cis*–*trans* switching is around 0.5 eV for low-coverage conditions where the switching is not affected by interactions from nearby RS–Au–SR complexes. The low activation barrier implies facile *cis*–*trans* isomerization at typical temperatures (200–300 K) where thiolate-SAMs are formed. Both isomers are also typically found in the STM images of low- or intermediate-coverage phases (Fig. 3a). A weak attraction has been calculated for adjacent *trans*-complexes; also, the steric repulsion is minimized if adjacent complexes are both either in *(R,R)* or *(S,S) trans*-configuration. These two factors drive the self-assembly of the 'stripes' at low coverage.

Intermediate and full-monolayer thiolate coverage. At present it is not clear how the striped phase of methylthiolates transfers to intermediate coverage or full-monolayer SAMs. It is reasonable to expect that the facile *cis*–*trans* isomerization of RS–Au–SR units, their mobility, steric interactions and possible other gold–sulfur bonding motifs may all play a role. STM images have shown tetrameric units assembled from RS–Au–SR complexes at intermediate coverage, and coexistence of one-dimensional stripes with (3 × 4) and (3 × 4√3) phases at high coverage[54,55]. It is possible to construct a full monolayer coverage with *c*(4 × 2) superstructure consisting only of *trans*-or *cis*-RS–Au–SR units without any disorder (Fig. 4a). DFT computations have shown that an ordered structure, consisting of two non-equivalent *cis*-RS–Au–SR units per unit cell (structure **9** in Fig. 4a), is energetically preferred over the 'standard model' (monothiolate bridge-site binding) or any models involving other adatom–thiolate complexes or Au surface vacancies[56]. This structural model also minimizes the calculated surface Gibbs free energy when the thiolate adsorption is modelled from a fictitious reservoir of disulfides at a given temperature and pressure[6].

STM gives a local view on the structure of individual adsorbates or adsorbate complexes on the surface, offering many possibilities for direct comparison to DFT computations. Practically all the other experimental surface-sensitive techniques average information over a large surface area, making comparison to calculations more challenging. Interesting progress has been recently achieved in comparing DFT computations and measurements for the Au(4*f*) photoelectron binding energies, specifically the computed surface core-level shifts (SCLS) from various structural models to experimental SCLS data on methylthiolate-SAMs[57–59]. The observed binding energies of Au(4*f*) electrons in the surface region give information about the local coordination structure and 'oxidation state' of gold atoms in the surface/interface region. Clean Au(111) surface has been shown to exhibit a surface SCLS component of –0.34 eV with respect to bulk gold atoms[58]. On adsorption of methylthiolates up to the full (3 × √3*R*30°) monolayer coverage, the surface component changes to –0.22 eV, and an additional component at +0.34 eV shows up (Fig. 4b). Based on this, the observation was initially interpreted as supporting the adatom–monothiolate adsorption model (structure **2** in Fig. 4a) where the shift at +0.34 eV arises from the Au adatoms supporting the monothiolate[58]. A subsequent DFT study

evaluated the shifts for the Au atoms at the gold–thiolate interface using a few representative adsorption models (structures **1**, **2**, **9** and **10** in Fig. 4a)[57]. Bridge-bound monothiolate (structure **1**) and Au adatom–monothiolate complex (structure **2**) yield only negative shifts and cannot account for the observed large positive shift of +0.34 eV. The positive shift arises from the formally oxidized, linearly bound Au adatoms in the polymeric complex –RS–Au(I)–RS–Au(I)–RS– in structure **10** and in the RS–Au(I)–RS complex in structure **9** (Fig. 4b). Overall, structure **9** yields SCLS values that are in the best agreement with the experiment[58].

There is one possible caveat in interpretation of experimental data with a set of energy-optimized DFT-computed static structures, as dynamical thermal effects cannot be accounted for. Results from photoelectron diffraction and GIXRD on the $(3 \times \sqrt{3}R30°)$ phase of methylthiolate/Au(111) have been interpreted via DFT-based molecular dynamics simulations to show a dynamical equilibrium between bridge-site monothiolate adsorption (the 'standard model') and RS–Au–SR units where the thiolate-bridging Au atoms are lifted from the surface (111) layer, creating a vacancy there[60]. This model has been subsequently applied to interpret GIXRD data on the $c(4 \times 2)$ hexylthiolate/Au(111)[61]. Although energetically quite unfavourable according to $T = 0$ DFT computations (structure **10** in Fig. 4a), one can argue that thermal dynamic effects in chain–chain interactions (van der Waals attraction and steric repulsion), gauche defects in the alkyl-chain layer, defect dynamics in the Au surface layer and the possible interchanges in the Au–S bonding will create enough configurational dynamic entropy to decrease the free energy of this kind of interface to be competitive with a more ordered structure (such as **9** in Fig. 4). A disordered Au–S interface structure cannot be completely excluded based on comparison of the calculated and measured SCLS values (Fig. 4b), so a definite structural assignment of that interface at the full coverage of longer alkylthiolates remains an experimental–theoretical challenge. In the absence of well-tested classical force-field models for the Au–S interface, one has to rely on DFT computations where the inclusion of a realistic description of the weak van der Waals interaction between the (longer) alkyl chains will probably be the next necessary step, and a challenge in itself.

Thiolate-protected nanoclusters of gold

The landmark report[62] by Brust, Schiffrin and co-workers in 1994 opened a new era for synthesis of air-stable, electrochemically stable and thermally stable cluster compounds with tunable sizes and properties on the nanometre scale[8–12]. Later refinements of the method

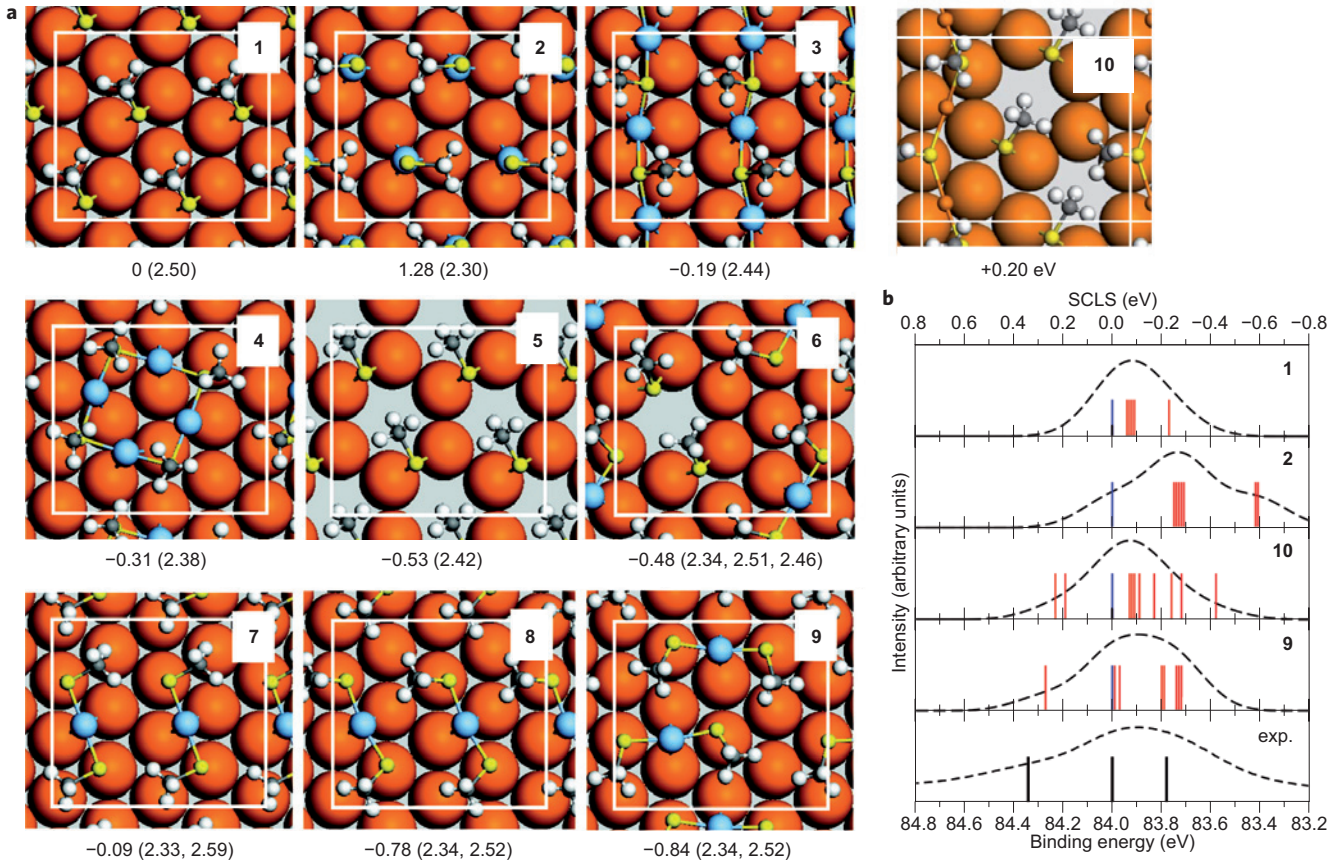

Figure 4 | DFT-optimized atomistic models for the saturation-coverage $c(4 \times 2)$ methylthiolate–gold interface and photoemission core-level shifts. **a**, Various structural models **1**–**9** have been considered, and the total energy per $c(4 \times 2)$ unit cell (the white rectangle) for all structures, with respect to the 'standard model' structure **1**, is reported in electron volts. The average Au–S distances (in Å) are shown in parenthesis. The Au adatom in structures **2**–**4** and **6**–**9** is shown in blue. An additional 'disordered' structure **10** has been proposed[61] from GIXRD experiments and molecular dynamics simulations for $c(4 \times 2)$ phase of hexylthiolate/Au(111) and methylthiolate/Au(111). Structure **10** includes a surface vacancy, two bridge-coordinated monothiolates and one polymeric –RS–Au–SR–Au– chain in the unit cell (the Au atoms in the chain are denoted by small orange spheres). Note that this configuration is endothermic by 0.2 eV with respect to the 'standard model' structure **1** in part **a**. **b**, Calculated Au(4*f*) surface core-level shifts (SCLS) and binding energies for the optimized structures **1**, **2**, **9** and **10**. Red bars denote the surface shifts and blue bars are the bulk components. The individual theoretical shifts are convoluted by a 0.3-eV Gaussian in order to compare to the experimental data (exp.) from ref. 58, de-convoluted through three SCLS components at shift values of +0.34 eV, 0 and –0.22 eV. Part **a** reproduced with permission from ref. 56, © 2008 ACS, part **b** reproduced with permission from ref. 57, © 2010 APS.

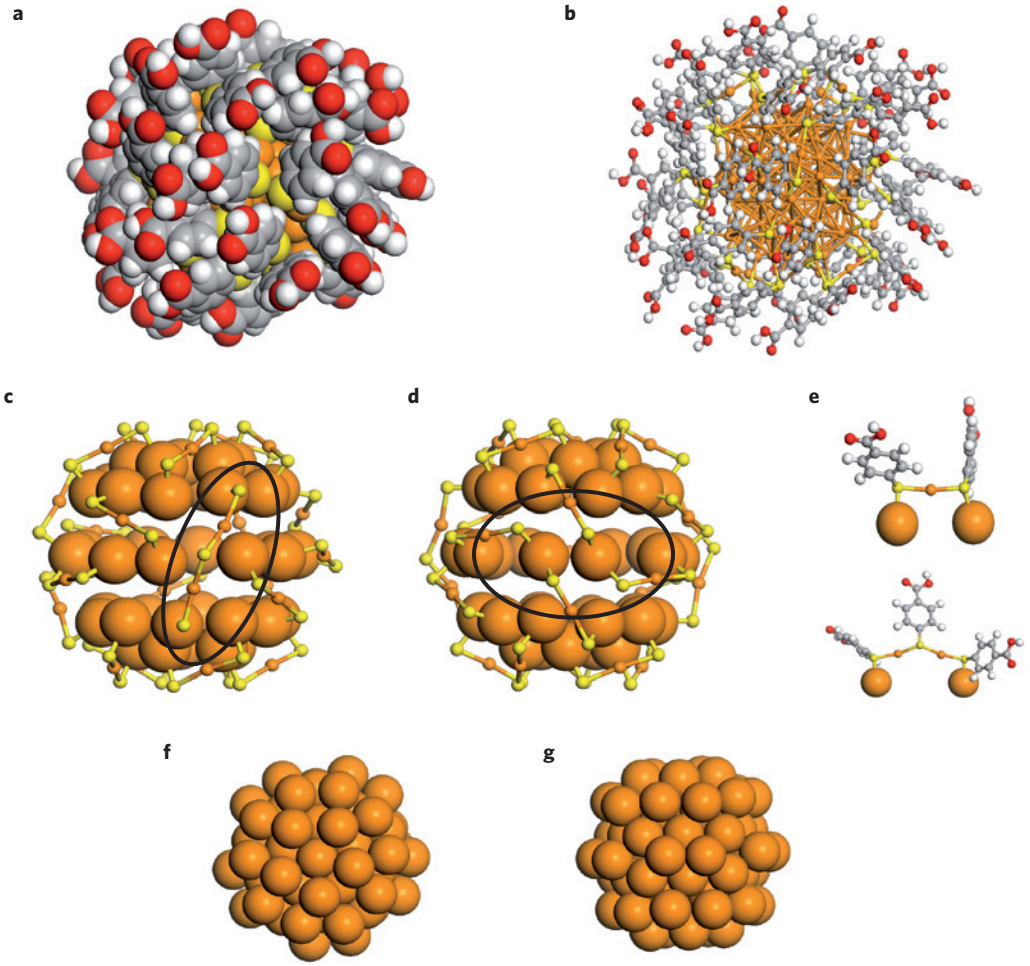

Figure 5 | Analysis of the single-crystal X-ray structure of *para*-mercaptobenzoic acid (*p*-MBA) protected cluster, $Au_{102}(p\text{-MBA})_{44}$. a, Space-filling and **b**, ball-and-stick representations. **c**,**d**, Two views of the 40-atom surface of the Au_{79} core, together with the passivating $Au_{23}(p\text{-MBA})_{44}$ mantle. The formally oxidized Au(I) atoms in the mantle are depicted by the smaller orange spheres. The 'structure defects' at the core–mantle interface (two Au atoms with two Au–S bonds, and a long RS–$(AuSR)_2$ unit) are highlighted. **e**, Close-up of the protecting RS–$(AuSR)_x$ unit with $x = 1,2$. **f**,**g**, Two views of the Au_{79} core, which has an approximate symmetry of D_{5h}. Au: orange; S: yellow; C: grey; O: red; H: white. Reproduced with permission from ref. 80, © 2008 NAS.

by several groups have enabled high-quality synthesis of a few particularly stable 'magic' compounds in the size range 1–3 nm, and a few have by now been determined up to molecular precision; these include $Au_{20}(SR)_{16}$ (ref. 63), $Au_{25}(SR)_{18}$ (refs 64–67), $Au_{38}(SR)_{24}$ (refs 68, 69), $Au_{40}(SR)_{24}$ (ref. 70), $Au_{68}(SR)_{34}$ (ref. 71), $Au_{102}(SR)_{44}$ (ref. 72), and compounds around 144 Au atoms and 60 thiolates[68,73,74]. Various thiolates have been successfully used for synthesis, including water-soluble glutathione and *para* mercaptobenzoic acid and organic-soluble alkylthiolates and phenylethanethiolates. The Au_{25}, Au_{38} and Au_{102} clusters are notable in this series because their total atomic structure has been determined from X-ray crystallography, opening the door to detailed theoretical analysis of the surface-covalent gold–sulfur bond and the electronic and geometric factors underlying the stability of these specific compounds.

It is now well established that the gold–sulfur interface in these clusters consists of oligomeric $RS(AuSR)_n$ units just like in the case of thiolate SAMs discussed above. This has revolutionized the understanding of the internal atomic structure of these systems and redefined the concepts of the 'metal core' and the 'passivating ligand layer'. At variance with early theoretical models that considered an atomically smooth Au–S interface and compact Au cores[75,76], Au atoms at the centre of the particle and in the thiolate layer are now considered to be in two distinct chemical states (metallic and oxidized). In fact, a more transparent way to write the molecular formula of the clusters is according to the 'divide and protect' notation[77] as follows: $Au_{25}(SR)_{18} = Au_{13}[RS(AuSR)_2]_6$; $Au_{38}(SR)_{24} = Au_{23}(RSAuSR)_3[RS(AuSR)_2]_6$; $Au_{102}(SR)_{44} = Au_{79}(RSAuSR)_{19}[RS(AuSR)_2]_2$ (Figs 5, 6, 7f,g). In addition, a structural model has been proposed[78] for the $Au_{144}(SR)_{60}$ cluster that gives a good match with the measured powder X-ray diffraction data. The model consists of a 114-atom gold core protected by 30 RSAuSR units (Fig. 6d–g). A similar model was recently proposed for mixed gold–silver $Au_{144-x}Ag_x(SR)_{60}$ clusters[79].

Because the neutral $RS(AuSR)_n$ units can be considered as radicals, simple electron-counting rules have been established that can successfully explain the electronic stability, that is, the origin of discrete HOMO–LUMO gaps in the electronic structure of thiolate-passivated clusters[10,80–82].

Chiral recognition and response

Chirality ('handedness') in the structure of matter is a fascinating property that has important consequences over a wide range of phenomena, properties and response of matter, relevant in the fields of physics, chemistry and life sciences[83]. Complex biological self-assembly processes are rooted in enantiospecific molecular interactions at the nanometre scale. Consequently it has been important to investigate the origins of enantiospecific molecular recognition to gain understanding of the underlying mechanisms that could be

used in developing nanoscale systems and devices for enantiospecific catalysis, sensing, optical activity or electronics, amongst other examples. Understanding the bonding at the gold–sulfur interface is relevant here as well.

A 'three-point contact' model has been a key concept in stereochemistry and pharmacology since the 1930s[84,85]. According to this model, enantiospecific molecular recognition is facilitated by binding of an incoming molecule to a receptor at three non-equivalent sites (Fig. 7d). STM experiments and DFT calculations have validated this model to some extent for adsorption of cysteine at an achiral Au(110) surface[86]. Cysteine is a chiral amino acid containing the thiol group that can make a covalent bond to gold via deprotonation. The other two non-equivalent (and non-covalent) interactions to gold are mediated through the amine and carboxyl groups. STM has shown ordering of homochiral (LL or DD) pairs of cysteine on Au(110) on adsorption from a racemic mixture, and the concomitant DFT calculations implied that the pairing is assisted by reorganization of Au atoms at the surface (Fig. 7a–c)[86].

As discussed above, RSAuSR units at the gold–sulfur interface have a chiral centre at each sulfur atom and the units can exist either in (*R*,*R*) / (*S*,*S*) *trans*-configuration or in (*R*,*S*) *cis*-configuration (Fig. 3). STM has shown self-assembly of the *trans*-RSAuSR units to homochiral [11$\bar{2}$] rows in case of propylthiolates; furthermore, neighbouring rows have alternating (*R*,*R*) and (*S*,*S*) chiralities (Fig. 7e)[55]. The enantiospecific packing is thought to arise from optimization of steric effects in the row and between the rows (Fig. 7e). This example demonstrates that enantiomeric separation can be achieved even in the case of an achiral support.

The origin of the circular dichroism of thiolate-protected gold nanoclusters has been debated for over a decade[87–98]. Chiroptical activity can be induced if chiral thiolates are used in the synthesis of gold clusters, if they are introduced to the clusters via ligand-exchange reactions as a post-synthesis step or if chiral phase transfer from a racemic solution is successful[87,88,90,91,94]. Theoretical studies have considered possibilities for geometrically chiral metal cores, chiral ligand footprint or dissymmetric ligand field models. One well-studied example is the gold–thiolate cluster compound known previously by its approximate core mass of 8 kDa, now believed to correspond to the known cluster $Au_{38}(SR)_{24}$. A decade ago, glutathione-protected Au_{38} was shown to yield intense circular dichroism signals at rather low excitation energies where the absorption is expected to be dominated by metal-based transitions (glutathione itself yields a circular dichroism signal but only at excitation energies over 5 eV)[87]. The recent experimental breakthrough in solving the crystal structure[68] of $Au_{38}(SCH_2CH_2Ph)_{24}$ and the computational discovery[99] of the origin of the optical activity of $Au_{38}(SCH_3)_{24}$ has shed light on this problem. Both the crystallographic structure and the computationally optimized structure of $Au_{38}(SR)_{24}$ show an achiral gold core of 23 atoms, protected by three RSAuSR and six $RS(AuSR)_2$ units (Fig. 7f). The geometrical arrangement of the nine gold–thiolate units has the chiral D_3 symmetry (Fig. 7f). This cluster yields a strong computed circular dichroism signal in the energy range up to 2.2 eV where the transitions are metal–metal or ligand–metal type (Fig. 7g). A geometrically closely related, but achiral, higher-energy C_{3h} isomer has a circular dichroism signal that is clearly weaker. These computational results indicate the important role of the chiral geometrical arrangement of the protecting gold–thiolate overlayer even though the metal core and the thiolate themselves can be achiral.

In the single-crystal experiment of $Au_{38}(SCH_2CH_2Ph)_{24}$ the crystal unit cell was observed to accommodate an enantiomeric pair of the clusters[68]. As the SCH_2CH_2Ph itself is achiral, enantiomeric separation of this cluster compound was a challenge that has been overcome only very recently, by using chiral high-performance liquid chromatography (HPLC)[98]. The measured circular dichroism signal from an enantiopure solution compares very well to the computations[99] for $Au_{38}(SCH_3)_{24}$.

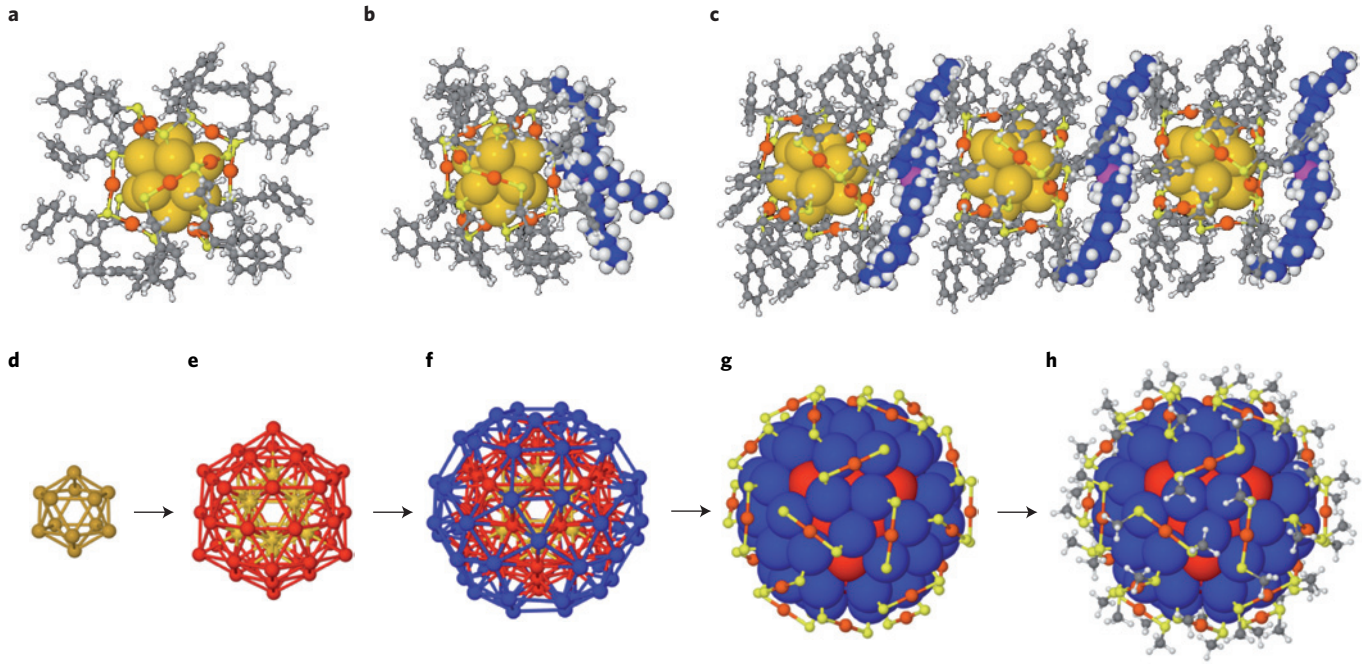

Figure 6 | Structures of the $Au_{25}(SR)_{18}^-$ and $Au_{144}(SR)_{60}$ clusters. a, Geometry of the $Au_{25}(SCH_2CH_2Ph)_{18}^-$ in the gas phase and **b**, together with the counterion TOA^+. **c**, Packing of the clusters and counterions in the crystal. The structures are computationally relaxed ones[131] with the initial structures taken from the known crystal structure data[65]. **d**–**f**, The concentric 12-atom (hollow), 42-atom and 60-atom Au shells of the 114-atom gold core of $Au_{144}(SCH_3)_{60}$, respectively. **g**, S–Au–S arrangement of the 30 RS–Au–SR units covering the surface (blue) of the 114-atom gold core; **h**, with all the atoms shown. Note the sphericity of the 60-atom gold rhombicosidodecahedron shell (blue) in part **f**. Parts **a**–**c** reproduced with permission from ref. 131, © 2010 ACS, parts **d**–**h** reproduced with permission from ref. 78, © 2009 ACS.

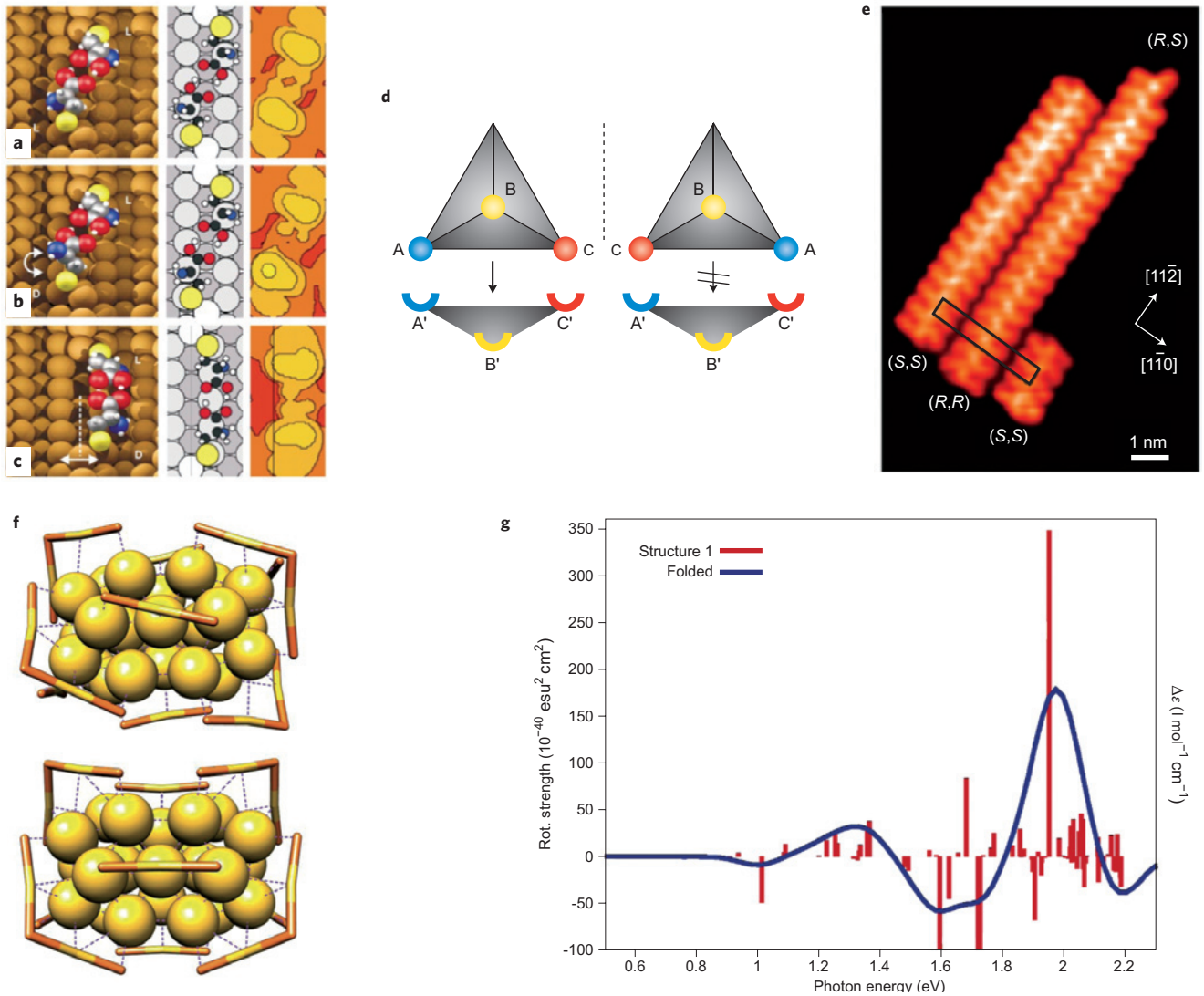

Figure 7 | Chiral recognition and response of organosulfur molecules at various gold surfaces. a–c, Atomic structure of cysteine pairs on Au(110) surface as obtained from DFT calculations (ref. 86) (left and middle columns) and the simulated STM images (right column). Pairing of L and D enantiomers is affected by three factors: (i) the tendency of sulfur to bridge two underlying Au atoms, inducing in some cases a local change of the surface reconstruction; (ii) interaction between the nitrogen lone pair and the gold surface; and (iii) the carboxylic acid dimerization. Together these form a 'three-point' contact for chiral recognition, visualized in part **d**. **e**, Striped phase of propylthiolate C_3H_7S on Au(111), formed by thermal deprotonation and subsequent self-assembly of propylthiols at $T > 250$ K. The stripes are formed by (*R*,*R*) and (*S*,*S*) *trans*-units of RSAuSR and packed according to alternating chiralities with a $(11 \times \sqrt{3})$ periodicity (the black rectangle denotes the unit cell). For the *R*,*S* notation specifying sulfur as the chiral centre and for the *cis*–*trans* notation see Fig. 3f,g. **f**, The Au–S framework in the computed structures (ref. 99) of the $Au_{38}(SR)_{24}$ cluster composed of an achiral Au_{23} core protected by three RS–Au–SR and six RS–Au–SR–Au–SR units. The units can be arranged in a chiral D_3 symmetry (top) or achiral C_{3h} symmetry (bottom). The chiral isomer is the energetic ground state and it has also been confirmed from single-crystal X-ray crystallography (ref. 69). **g**, Computed circular dichroism signal of the D_3 cluster with SR = SCH_3. Reproduced with permission from the respective sources: parts **a**–**d**, ref. 86, © 2002 NPG; **e**, ref. 55, © 2009 ACS, **f**,**g**, ref. 99, © 2010 ACS.

Gold–thiolate molecular junctions

Single, well-defined molecule–metal junctions have, since the 1970s, been envisaged as cheap, fast and robust building blocks for electronic devices[100–104]. Gold–sulfur bonding has played a central role in this field, as the thiol group is frequently used to link various organic molecules covalently to metal electrodes, which usually are made of gold. Alkylthiolates and derivatives of π-conjugated arylthiolates have 'intrinsic' conductivities that can be expected to differ by several orders of magnitude. The true challenge is the molecular-scale control of the number and geometry of the 'molecular wires' in the junction between the electrodes.

A pioneering experiment, published in 1997, attempted to form and measure the conductance of a single-molecule junction consisting of a benzene-1,4-dithiol (BDTH, HSPhSH; Ph = phenyl) molecule between gold electrodes at room temperature[105]. The experiment made use of the so-called mechanically controllable break junction technique, where a notched gold wire was immersed in a solution containing the BDTH. The contact was broken in the solution, leading to formation of a SAM of BDT molecules (that is, as thiolate, SPhS) on the electrodes. The solvent was then allowed to evaporate, and the system was kept in argon atmosphere for measurements. The electrodes were subsequently brought together and separated several times, and the current–voltage (I–V) characteristics of the junction were recorded. At an electrode separation of about 8 Å, stable contacts were formed such that their I–V characteristics could be determined reproducibly. A

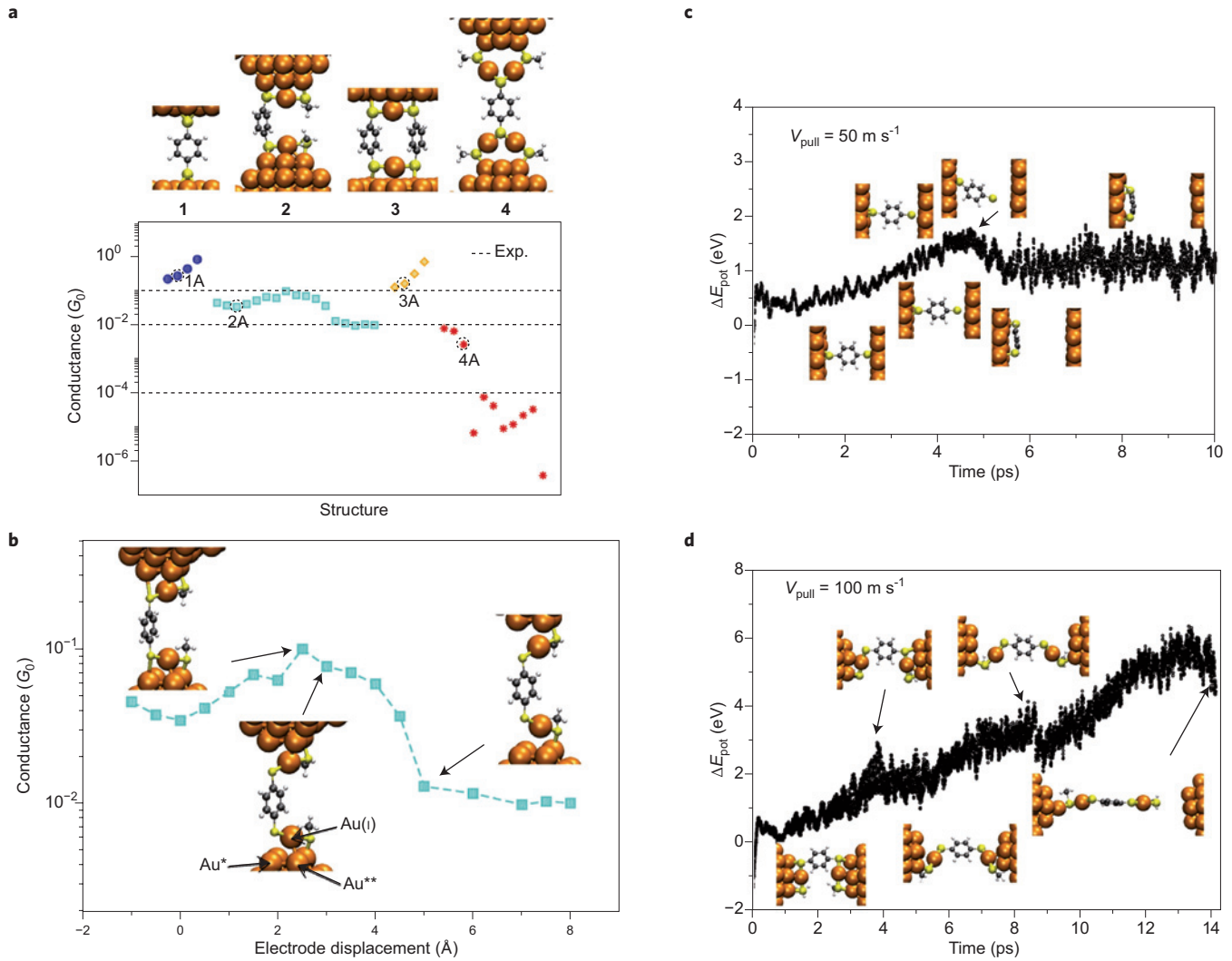

Figure 8 | Schematics of Au–BDT–Au junctions and computed structures, conductance and dynamics by using the novel RS(AuSR)$_n$ motif. **a**, Equilibrium structures of four model junctions **1**–**4** at mechanical equilibrium (top) and their conductance values as the junctions are manipulated (bottom). The values at the mechanical equilibrium are labelled 1A to 4A. The horizontal dashed lines denote various conductance values G (or ranges of G) reported from experiments. **b**, Conductance of **2** as a function of the electrode displacement, with the mechanical equilibrium at 0. The insets from left to right highlight important structural changes occurring during the elongation, correlating with the conductance data. Left: maximal strain of the S–Au* bond corresponding to the maximal G; middle: breaking of the S–Au* bond reflected in an immediate drop of G and subsequent elongation and breaking of the Au(I)–Au** bond; right: G settles to a value of about $0.1G_0$ after the Au(I)–Au** bond is broken. Further elastic stretching of the long molecular wire, containing both Au(I) atoms, does not affect G, because the BDT moiety is electronically decoupled from the electrodes. **c**, Time evolution of the potential energy (E_{pot}) of junction **1** in DFT molecular dynamics simulation (pulling speed 50 m s^{-1}). **d**, The corresponding data for junction **2** (pulling speed 100 m s^{-1}). Note the 'tumbling back' of BDT after junction rupture in **c** and re-bonding parallel to the Au(111) surface. Reproduced with permission from ref. 121, © 2010 ACS.

central plateau in the I–V curve (0.7 eV) and two values of contact resistance were determined, about 22.2 MΩ and 13.3 MΩ, which correspond to conductance values of $5.8 \times 10^{-4}G_0$ and $9.7 \times 10^{-4}G_0$, respectively, in units of the conductance quantum $G_0 = 2e^2/h$. Because the size of the BDT molecule roughly corresponds to the gap determined between the gold electrodes, it was concluded that: "The reproducibility of the minimum conductance at a consistent value implies that the number of active (BDT) molecules could be as few as one"[105].

It is obvious that the measured resistance of the junction is intimately related to the total geometry of the molecule(s) and sulfur–gold interface, and it was found later in numerous experiments that an unambiguous determination of a (single) 'conductance' value even for the conceptually rather simple Au–BDT–Au junction is truly challenging[106–115]. After the first experiment, a wide variety of conductance values ($10^{-4}G_0$ to $0.5G_0$) for this junction, generated either by contacting and retracting an STM tip, or by using the mechanically controllable break junction set-up, has been found, as shown schematically in Fig. 8a. This is currently understood as arising from the variations in the experimental geometries, set-ups and measurement protocols. Crucial factors are the initial density of the partial thiol(ate) coverage on the electrodes, whether the electrodes are driven to full metallic contact (having conductance of several quantum units) before subsequent retraction and break-up, and whether thiol molecules are available to migrate into the broken contact at each cycle. Statistical measurements have also shown temperature effects in the range of typical measurement temperatures between a few tens of kelvin and room temperature.

The wide scatter of experimental data has created challenges to theory and computations[116–125]. Treatments based on DFT or

semi-empirical tight-binding models have shown that the coordination of the sulfur to the gold surface (top, bridge, hollow sites), the orientation of the phenyl ring with respect to the crystallographic orientation of the electrodes, the detailed combined electronic structure of the molecule–metal contact including proper screening effects, and the dynamical effects all play an important role in modifying the conductance. But no unambiguous agreement currently exists between theory and experiment, making the situation puzzling.

It is essential to realize, however, that all computations but one[121] have so far considered a very idealized junction geometry, namely that of the BDT-terminating sulfur coordinating to a locally smooth Au(111) surface or on an apex of a pyramidal tip structure. In the light of the current knowledge of the Au–S interface of Au(111)/SAMs and of thiolate-protected gold nanoclusters, it is conceivable that RS–(Au(I)–SR)$_n$ units exist at the highly curved tips of the electrodes. As discussed above, these units have been experimentally detected for both low-coverage and high-coverage SAMs and on a 'curved' SAM interface of the nanoclusters. In fact, any of the crystallographically known nanometre-sized Au$_n$(SR)$_m$ clusters ((*n*,*m*) = (25,18), (38,24), (102,44)) could offer a realistic model for the thiolated tip apex of the electrodes. The relevant question is then what happens to the RS–(Au(I)–SR)$_n$ overlayer units during repeated contacting and retracting of the electrodes. Unfortunately, direct DFT-based molecular dynamics simulations are currently prohibitively intensive in computing time, and realistic classical force field models are lacking (acceptable classical force fields need to be able to describe Au–SR bond-breaking energetics and dynamics with the accuracy of the full DFT).

Only one recent computational study has so far considered the possibility of the interacting RS–(Au(I)–SR)$_n$ units at the opposing electrode surfaces[121]. A few model structures for these novel junctions (**2**–**4**) and their conductance values, calculated by Green's function methods, are shown in Fig. 8a and compared with the 'standard model' **1**, shown schematically also in Fig. 1. The equilibrium structures of **1**–**4** span a wide variety of conductance values between $2.8 \times 10^{-1}G_0$ and $8 \times 10^{-3}G_0$. The more interesting point of comparison with experiments is to consider these junctions under tension, because from statistical measurements, the determined 'conductance values' are drawn from the peaks (if any) in the conductance distribution corresponding to plateaux in conductance versus stretching curves. Junctions **2** and **4** show very interesting behaviour: **2** gives a plateau at about $0.01G_0$ and **4** settles to scattering values below $10^{-4}G_0$. Both junctions can be stretched considerably, by more than 1 nm, from their equilibrium geometry. For instance, the DFT molecular dynamics simulations of **2** show a clear formation of a long contact Au(electrode)–SR–Au(I)–SPhS–Au(I)–RS–Au(electrode) before rupture (Fig. 8b,d). The 'molecular wire' that yields the conductance plateau at about $0.01G_0$ is then the long complex –SR–Au(I)–SPhS–Au(I)–RS–. It is crucial to realise that the two Au(I) atoms in the wire are chemically in a distinctly different state from the Au(0) atoms at the surface of the metal electrode. This applies also when these atoms are closer to the electrodes in the mechanical equilibrium. The Au(I) atoms also play a role in passivating the sulfurs of the central BDT moiety; this has important consequences for the conducting orbitals of the BDT[121,125]. The calculations confirm the experimental and many earlier theoretical results that the measured conductance is mainly due to one conducting state of BDT, but its resonance position and shape close to the Fermi energy are very sensitive to the electronic structure of the sulfurs. State-of-art *GW* methods, considering just the simple 'standard model' **1**, give similar conductance values to junction **2** (calculated from the Green's function method) if the sulfurs in **1** are passivated by hydrogens[125]. On the other hand, the standard model junction **1** is much stiffer than **2** against stretching, the conductance increases even close to $1G_0$ before breaking (Fig. 8a) and on breaking the BDT molecule tumbles back and binds parallel to the Au(111) surface of one of the electrodes (Fig. 8c). It is clear that further computational work is needed to evaluate many other possible geometries of the junctions containing the novel gold–thiolate units, and eventually molecular dynamics simulations should be performed for the improved geometry models to determine statistics of the conductance plateaux. This poses a considerable computational challenge for the coming years.

Conclusion and outlook

Tremendous progress has been achieved during the past five years, both on the experimental and the theoretical fronts, in understanding the molecular structure of the gold–sulfur nanometre-scale interface in thiolate-SAMs on Au(111) and in thiolate-protected gold nanoclusters. Formation of the polymeric –RS–Au(I)–SR– units and the existence of two chemical states of gold (Au(0) and Au(I)) are by now well-established features of that interface, and they can be expected to be important for understanding atomistic mechanisms of, for example, ligand-exchange reactions, dynamical stability and catalytic activity of protected gold nanoclusters[126], or local roughness of SAM surfaces[127].

Despite all the advances discussed in this Review, a few open issues remain regarding thiolate-stabilized clusters. Appearance of the 'magic' sizes (*n*,*m*) for Au$_n$(SR)$_m$ clusters is affected both by thermodynamics and kinetics, as has been elegantly shown in the case of glutathione-stabilized clusters[64]. Although the synthesis yields appreciable amounts of a series of (*n*,*m*) clusters such as (10,10), (11,11), (12,12), (15,13), (18,14), (22,16), (22,17), (25,18), (29,20), (33,22), (35,22), (38,24), (39,24), most of them decay on a timescale of a few days either to polymeric (*n*,*n*) forms or into (25,18) and (38,24) clusters, which thus seem to be the thermodynamically stable compositions in this size region. It is clear that only a few of the observed (*n*,*m*) compositions can be explained from an electronic structure point of view as electron shell closures[10,80], so structural effects must play a part as well. For the larger sizes, it seems that the stability of the (144,60) compound can well be explained solely by geometric effects. In fact the proposed (144,60) icosahedral structure[78] has recently been suggested as the 'core structure' for larger icosahedral-based plasmonic clusters with approximate composition of about 330 Au atoms and 80 thiolates (76 kDa mass)[128,129].

In the coming years, the use of monothiol(ate)- or dithiol(ate)-stabilized gold nanoclusters for bio-applications is expected to increase. In this area, they have already been demonstrated for contrast enhancement in electron microscopy, delivery and enhancement of existing small molecule drugs, and as intrinsically pharmaceutically active compounds. A better understanding of the role of the Au–S interface for long-term stability of gold nanoclusters in living cells, under the influence of bio-thiols such and glutathione and cysteine[130], may then be crucial for successful use of gold-based agents for biolabelling, drug delivery and photothermal therapy. Understanding the very fine details of the internal structure and stability of the organic thiolate ligand shell is expected to be crucial for the control of ligand-exchange reactions that are at the heart of the bio-functionalization of the nanoparticle surface. The large number of distinctly different kinetic environments for ligand-exchange for some known Au:SR clusters raises the possibility of treating these systems analogously to proteins, which have a distinct three-dimensional sequence of amino acids that can be routinely modified by protein engineering, or analogously to DNA, which can be modified by site-directed mutagenesis.

Model calculations[121] have now shown that the Au(I) atoms have a distinct role also for transmitting electrical current through Au–S nanojunctions, because they may form an integral part of the

'molecular nanowire'. Much more work is, however, needed in this area to establish the structure of the most robust junctions that are formed under various experimental conditions. The structures discussed in this Review may be most relevant for experiments where the metal contacts are formed and broken in thiol solutions, where a full SAM on the gold tips can be expected to form in each contact cycle. Formation of the oligomeric gold–sulfur units is a manifestation of the strong chemical modification of gold electrodes by thiolates, and its effects for the electrical contact also need to be carefully re-evaluated in situations where individual biomolecules make contact to gold electrodes through thiolate linkers.

References

1. Dubois, L. H. & Nuzzo, R. G. Synthesis, structure, and properties of model organic surfaces. *Annu. Rev. Phys. Chem.* **43,** 437–463 (1992).
2. Ulman, A. Formation and structure of self-assembled monolayers. *Chem. Rev.* **96,** 1533–1554 (1996).
3. Schreiber, F. Structure and growth of self-assembling monolayers. *Prog. Surf. Sci.* **65,** 151–256 (2000).
4. Love, J. C., Estroff, L. A., Kriebel, J. K., Nuzzo, R. G. & Whitesides, G. M. Self-assembled monolayers of thiolates on metals as a form of nanotechnology. *Chem. Rev.* **105,** 1103–1169 (2005).
5. Woodruff, D. P. The interface structure of *n*-alkylthiolate self-assembled monolayers on coinage metal surfaces. *Phys. Chem. Chem. Phys.* **10,** 7211–7221 (2008).
6. Vericat, C., Vela, M. E., Benitez, G., Carro, P. & Salvarezza, R. C. Self-assembled monolayers of thiols and dithiols on gold: new challenges for a well-known system. *Chem. Soc. Rev.* **39,** 1805–1834 (2010).
7. Maksymovych, P., Voznyy, O., Dougherty, D. B., Sorescu, D. C. & Yates, J. T. Gold adatom as a key structural component in self-assembled monolayers of organosulfur molecules on Au(111). *Prog. Surf. Sci.* **85,** 206–240 (2010).
8. Templeton, A. C., Wuelfing, W. P. & Murray, R. W. Monolayer-protected cluster molecules. *Acc. Chem. Res.* **33,** 27–36 (2000).
9. Daniel, M-C. & Astruc, D. Gold nanoparticles: assembly, supramolecular chemistry, quantum-size-related properties, and applications toward biology, catalysis and nanotechnology. *Chem. Rev.* **104,** 293–346 (2004).
10. Häkkinen, H. Atomic and electronic structure of gold clusters: understanding flakes, cages and superatoms from simple concepts. *Chem. Soc. Rev.* **37,** 1847–1859 (2008).
11. Sardar, R., Funston, A. M., Mulvaney, P. & Murray, R. W. Gold nanoparticles: past, present and future. *Langmuir* **25,** 13840–13851 (2009).
12. Jin, R. Quantum sized, thiolate-protected gold nanoclusters. *Nanoscale* **2,** 343–362 (2010).
13. Ratner, M. A. Introducing molecular electronics. *Mater. Today* **5,** 20–27 (2002).
14. Agraït, N., Yeyati, A-L. & van Ruitenbeek, J.-M. Quantum properties of atomic-sized conductors. *Phys. Rep.* **377,** 81–279 (2003).
15. Nitzan, A. & Ratner, M. A. Electron transport in molecular wire junctions. *Science* **300,** 1384–1389 (2003).
16. Chen, F & Tao, N. J. Electron transport in single molecules: from benzene to graphene. *Acc. Chem. Res.* **42,** 429 (2009).
17. Ackerson, C. J., Powell, R. D. & Hainfeld, J. F. in *Cryo-EM Part A: Sample Preparation and Data Collection. Methods in Enzymology* Vol. 481 (Elsevier, 2010).
18. Ackerson, C. J., Jadzinsky, P. D., Sexton, J. Z., Bushnell, D. A. & Kornberg, R. D. Synthesis and bioconjugation of 2 and 3 nm-diameter gold nanoparticles. *Bioconjugate Chem.* **21,** 214–218 (2010).
19. Bowman, M-C. *et al.* Inhibition of HIV fusion with multivalent gold nanoparticles. *J. Am. Chem. Soc.* **103,** 6896 (2008).
20. Giljohann, D. A. *et al.* Gold nanoparticles for biology and medicine. *Angew. Chem. Int. Ed.* **49,** 3280 (2010).
21. Verma, A. & Stellacci, F. Effect of surface properties on nanoparticle–cell interactions. *Small* **6,** 12–21 (2010).
22. Demers, L. M. *et al.* Direct patterning of modified oligonucleotides on metals and insulators by dip-pen nanolithography. *Science* **296,** 1836 (2002).
23. Whetten, R. L. & Price R. C. Nano-golden order. *Science* **318,** 407–408 (2007).
24. Puddephatt, R. J. *The Chemistry of Gold* (Elsevier, 1978).
25. Schmidbaur, H. (ed.) *Gold: Progress in Chemistry, Biochemistry and Technology* (Wiley, 1999).
26. Laguna, A. (ed) *Modern Supramolecular Gold Chemistry* (Wiley, 2008).
27. Shaw, C. F. Gold-based therapeutic agents. *Chem. Rev.* **99,** 2589–2600 (1999).
28. Dance, I. G. The structural chemistry of metal thiolate complexes. *Polyhedron* **5,** 1037–1104 (1986).
29. Wilson, R. The use of gold nanoparticles in diagnostics and detection. *Chem. Soc. Rev.* **37,** 2028–2045 (2008).
30. Rawlings, D. E. Heavy metal mining using microbes. *Annu. Rev. Microbiol.* **56,** 65–91 (2002).
31. Wiseman, M. R., Marsh, P. A., Bishop. P. T., Brisdon, B. J. & Mahon, M. F. Homoleptic gold thiolate catenanes. *J. Am. Chem. Soc.* **122,** 12598 (2000).
32. Bau, R. Crystal structure of the antiarthritic drug gold thioamalate (myochrysine): a double helical geometry in the solid state. *J. Am. Chem. Soc.* **120,** 9380 (1998).
33. Pyykkö, P. Relativistic effects in structural chemistry. *Chem. Rev.* **88,** 563–594 (1988).
34. Pyykkö, P. & Desclaux, J. P. Relativity and the periodic system of elements. *Acc. Chem. Res.* **12,** 276–281 (1979).
35. Grönbeck, H. Walter, M. & Häkkinen, H. Theoretical characterization of cyclic thiolated gold clusters. *J. Am. Chem. Soc.* **128,** 10268–10275 (2006).
36. Howell, J. A. S. Structure and bonding in cyclic thiolate complexes of copper, silver and gold. *Polyhedron* **25,** 2993–3005 (2006).
37. Shao, N., Pei, Y., Gao, Y. & Zheng, X. C. Onset of double helical structure in small-sized homoleptic gold thiolate clusters. *J. Phys. Chem. A* **113,** 629–632 (2009).
38. Kacprzak, K. A., Lopez-Acevedo, O.;, Häkkinen, H. & Grönbeck, H. Theoretical characterization of cyclic thiolated copper, silver and gold clusters. *J. Phys. Chem. C* **114,** 13571–13576 (2010).
39. Barngrover, B. M. & Aikens, C. M. Incremental binding energies of gold(I) and silver(I) thiolate clusters. *J. Phys. Chem. A* **115,** 11818–11823 (2011).
40. Ning, C-G., Xiong, X-G., Wang, Y-L., Li, J. & Wang, L-S. Probing the electronic structure and chemical bonding of the 'staple' motifs of thiolate gold nanoparticles: $Au(SCH_3)_2^-$ and $Au_2(SCH_3)_3^-$. *Phys. Chem. Chem. Phys.* (in the press).
41. Henkelman, G., Arnaldsson, A. & Jonsson, H. A fast and robust algorithm for Bader decomposition of charge density. *Comput. Mater. Sci.* **36,** 354–360 (2006).
42. Nuzzo, R.G & Allara, D. L. Adsorption of bifunctional organic disulfides on gold surfaces. *J. Am. Chem. Soc.* **105,** 4481–4483 (1983).
43. Nuzzo, R. G., Zegarski, B. R. & Dubois, L. H. Fundamental studies of the chemisorption of organosulfur compounds on gold(111). Implications for molecular self-assembly on gold surfaces. *J. Am. Chem. Soc.* **109,** 733–740 (1987).
44. Chidsey, C. E. D., Liu, G. Y., Rowntree, P. & Scoles, G. Molecular order at the surface of an organic monolayer studied by low energy helium diffraction. *J. Chem. Phys.* **91,** 4421 (1989).
45. Strong, L. & Whitesides G. M. Structures of self-assembled monolayer films of organosulfur compounds adsorbed on gold single crystals: electron diffraction studies. *Langmuir* **4,** 546–558 (1988).
46. Chidsey, C. E. D. & Loiacono, D. N. Chemical functionality in self-assembled monolayers: structural and electrochemical properties. *Langmuir* **6,** 682–691 (1990).
47. Fenter, P., Eberhardt, A. & Eisenberger, P. Self-assembly of N-alkyl thiols as disulfides on Au(111). *Science* **266,** 1216–1218 (1994).
48. Fenter, P. *et al.* On the structure and evolution of the buried S/Au interface in self-assembled monolayers: X-ray standing wave results. *Surf. Sci.* **412/413,** 213–215 (1998).
49. Kondoh, H. *et al.* Adsorption of thiolates to singly coordinated sites on Au(111) evidenced by photoelectron diffraction. *Phys. Rev. Lett.* **90,** 066102 (2003).
50. Roper, M. G. *et al.* Atop adsorption site of sulfur head groups in gold–thiolate self-assembled monolayers. *Chem. Phys. Lett.* **389,** 87–91 (2004).
51. Molina. L. M. & Hammer, B. Theoretical study of thiol-induced reconstructions on the Au(111) surface. *Chem. Phys. Lett.* **360,** 264–271 (2002).
52. Maksymovych, P., Sorescu, D. C. & Yates, J. T. Jr Gold-adatom-mediated bonding in self-assembled short-chain alkanethiolate species on the Au(111) surface. *Phys. Rev. Lett.* **97,** 146103 (2006).
53. Maksymovych, P. & Yates, J. T. Au adatoms in self-assembly of benzenethiol on the Au(111) surface. *J. Am. Chem. Soc.* **130,** 7518–7519 (2008).
54. Voznyy, O. & Dubowski, J. J. $c(4 \times 2)$ structures of alkanethiol monolayers on Au(111) compatible with the constraint of dense packing. *Langmuir* **25,** 7353–7358 (2009).
55. Voznyy, O., Dubowski, J. J., Yates, J. T. & Maksymovych, P. The role of gold adatoms and stereochemistry in self-assembly of methylthiolate on Au(111). *J. Am. Chem. Soc.* **131,** 12989–12993 (2009).
56. Grönbeck, H., Häkkinen, H. & Whetten, R. L. Gold-thiolate complexes form a unique $c(4 \times 2)$ structure on Au(111). *J. Phys. Chem. C* **112,** 15940–15942 (2008).
57. Grönbeck, H. & Odelius, M. Photoemission core-level shifts reveal thiolate–Au(111) interface. *Phys. Rev. B* **82,** 085416 (2010).
58. Chaudhuri, A., Lerotholi, T. J., Jackson, D. C., Woodruff, D. P. & Dhanak, V. Local methylthiolate adsorption geometry on Au(111) from photoemission core-level shifts. *Phys. Rev. Lett.* **102,** 126101 (2009).

59. Chaudhuri, A., Lerotholi, T. J., Jackson, D.C, Woodruff, D. P. & Dhanak, V. R. The local adsorption structure of methylthiolate and butylthiolate on Au(111): A photemission core-level shift investigation. *Surf. Sci.* **604,** 227 (2010).
60. Mazzarello, R. *et al.* Structure of a CH3S monolayer on Au(111) solved by the interplay between molecular dynamics calculations and diffraction measurements. *Phys. Rev. Lett.* **98,** 016102 (2007).
61. Cossaro, A. *et al.* X-ray diffraction and computation yield the structure of alkanethiols on gold(111). *Science* **321,** 943–946 (2008).
62. Brust, M., Walker, M., Bethell, D., Schiffrin, D. J. & Whyman, R. Synthesis of thiol-derivatized gold nanoparticles in a 2-phase liquid–liquid system. *Chem. Commun*. 801–802 (1994).
63. Zhu, M. Z., Qian, H. F. & Jin, R. C. Thiolate-protected Au_{20} clusters with a large energy gap of 2.1 eV. *J. Am. Chem. Soc.* **131,** 7220 (2009).
64. Negishi, Y., Nobusada, K. & Tsukuda, T. Glutathione-protected gold clusters revisited: Bridging the gap between gold(I)-thiolate complexes and thiolate-protected gold nanocrystals. *J. Am. Chem. Soc.* **127,** 5261–5270 (2005).
65. Heaven, M. W., Dass, A., White, P. S., Holt, K. M. & Murray, R. W. Crystal structure of the gold nanoparticle $[N(C_8H_{17})_4][Au_{25}(SCH_2CH_2Ph)_{18}]$. *J. Am. Chem. Soc*. **130,** 3754–3755 (2008).
66. Zhu, M., Aikens, C. M., Hollander, F. J., Schatz, G. C. & Jin, R. C. Correlating the crystal structure of a thiol-protected Au_{25} cluster and optical properties. *J. Am. Chem. Soc*. **130,** 5883–5885 (2008).
67. Zhu, M., Eckenhoff, W. T., Pintauer, T. & Jin, R. C. Conversion of anionic $[Au_{25}(SCH_2CH_2Ph)_{18}]^-$ cluster to charge neutral cluster via air oxidation *J. Phys. Chem. C* **112,** 14221–14224 (2008).
68. Chaki, N. K., Negishi, Y., Tsunoyama, H., Shichibu, Y. & Tsukuda, T. Ubiquitous 8 and 29 kDa gold:alkanethiolate cluster compounds: mass-spectrometric determination of molecular formulas and structural implications. *J. Am. Chem. Soc.* **130,** 8608–8610 (2008).
69. Qian, H. F., Eckenhoff, W. T., Zhu, Y., Pintauer, T. & Jin, R. C. Total structure determination of thiolate-protected Au_{38} nanoparticles. *J. Am. Chem. Soc.* **132,** 8280–8281 (2010).
70. Qian, H. F., Zhu, Y. & Jin, R. C. Isolation of ubiquitous $Au_{40}(SR)_{24}$ clusters from the 8 kDa gold clusters. *J. Am. Chem. Soc.* **132,** 4583–4585 (2010).
71. Dass, A. Mass spectrometric identification of $Au_{68}(SR)_{34}$ molecular gold nanoclusters with 34-electron shell closing. *J. Am. Chem. Soc.* **131,** 11666–11667 (2009).
72. Jadzinsky, P. D., Calero, G., Ackerson, C. J., Bushnell, D. A. & Kornberg, R. D. Structure of a thiol monolayer-protected gold nanoparticle at 1.1 Å resolution. *Science* **318,** 430–433 (2007).
73. Fields-Zinna, C. A., Sardar, R., Beasley, C. A. & Murray, R. W. Electrospray ionization mass spectrometry of intrinsically cationized nanoparticles $Au_{144/146}(SC_{11}H_{22}N(CH_2CH_3)_3^+)_x(S(CH_2)_5CH_3)_y]^{x+}$. *J. Am. Chem. Soc.* **131,** 16266–16271 (2009).
74. Qian, H. F. & Jin, R. C. Controlling nanoparticles with atomic precision: the case of $Au_{144}(SCH_2CH_2Ph)_{60}$. *Nano Lett.* **9,** 4083–4087 (2009).
75. Häkkinen, H., Barnett, R. N. & Landman, U. Electronic structure of passivated $Au_{38}(SCH_3)_{24}$ nanocrystal. *Phys. Rev. Lett.* **82,** 3264–3267 (1999).
76. Garzon, I. L. *et al.* Do thiols merely passivate gold nanoclusters? *Phys. Rev. Lett.* **85,** 5250–5251 (1999).
77. Häkkinen, H., Walter, M. & Grönbeck, H. Divide and protect: capping gold nanoclusters with molecular gold-thiolate rings. *J. Phys. Chem. B* **110,** 9927–9931 (2006).
78. Lopez-Acevedo, O., Akola, J., Whetten, R. L., Grönbeck, H. & Häkkinen, H. Structure and bonding in the ubiquitous icosahedral metallic gold cluster $Au_{144}(SR)_{60}$. *J. Phys. Chem. C* **113,** 5035–5038 (2009).
79. Malola, S. & Häkkinen, H. Electronic structure and bonding of icosahedral core–shell gold–silver nanoalloy clusters $Au_{144-x}Ag_x(SR)_{60}$. *J. Phys. Chem. Lett.* **2,** 2316–2321 (2011).
80. Walter, M. *et al.* A unified view of ligand-protected gold clusters as superatom complexes. *Proc. Natl Acad. Sci.* **105,** 9157–9162 (2008).
81. Akola, J., Walter, M., Whetten, R. L., Häkkinen, H. & Grönbeck, H. On the structure of thiolate-protected Au_{25}. *J. Am. Chem. Soc.* **130,** 3756–3757 (2008).
82. Hulkko, E. *et al.* Electronic and vibrational signatures of the $Au_{102}(pMBA)_{44}$ cluster. *J. Am. Chem. Soc.* **133,** 3752 (2011).
83. Amabilino, D. B. (ed.) *Chirality at the Nanoscale* (Wiley, 2009).
84. Easson, E. H. & Stedman, E. Studies on the relationship between chemical constitution and physiological action. Molecular dissymmetry and physiological activity. *Biochem. J.* **27,** 1257 (1933).
85. Booth, T. D., Wahnon, D. & Wainer, I. W. Is chiral recognition a three-point process? *Chirality* **9,** 96–98 (1997).
86. Kühnle, A., Linderoth, T. R., Hammer, B. & Besenbacher, F. Chiral recognition in dimerization of adsorbed cysteine observed by scanning tunnelling microscopy. *Nature* **415,** 891–893 (2002).
87. Schaaff, T. G. & Whetten, R. L. Giant gold–glutathione cluster compounds: intense optical activity in metal-based transitions. *J. Phys. Chem. B* **104,** 2630–2641 (2000).
88. Yanagimoto, Y, Negishi, Y., Fujihara, H. & Tsukuda, T. Chiroptical activity of BINAP-stabilized undecagold clusters. *J. Phys. Chem. B* **110,** 11611–11614 (2006).
89. Goldsmith, M-R. *et al.* The chiroptical signature of achiral metal clusters induced by dissymmetric adsorbates. *Phys. Chem. Chem. Phys.* **8,** 63–67 (2006).
90. Yao, H., Fukui, T. & Kimura K. Chiroptical response of D/L penicillamine-capped gold clusters under perturbations of temperature change and phase transfer. *J. Phys. Chem. C* **111,** 14968 (2007).
91. Yao, H., Fukui, T. & Kimura K. Asymmetric transformation of monolayer-protected gold nanoclusters via chiral phase transfer. *J. Phys. Chem. C* **112,** 16281 (2008).
92. Qi, H. & Hegmann, T. Postsynthesis racemization and place exchange reactions. Another step to unravel the origin of chirality for chiral ligand-capped gold nanoparticles. *J. Am. Chem. Soc.* **130,** 14201–14206 (2008).
93. Noguez, C. & Garzon, I. L. Optically active metal nanoparticles. *Chem. Soc. Rev.* **38,** 757 (2009).
94. Si, S., Gautier, C., Boudon, J., Taras, R., Gladiali, S. & Burgi, T. Ligand exchange on Au_{25} cluster with chiral thiols. *J. Phys. Chem. C* **113,** 12966 (2009).
95. Gautier, C. & Burgi, T. Chiral gold nanparticles. *ChemPhysChem* **10,** 483–492 (2009).
96. Sanchez-Castillo, A., Noguez, C. & Garzon, I. L. On the origin of the optical activity displayed by chiral-ligand-protected metallic nanoclusters. *J. Am. Chem. Soc.* **132,** 1504 (2010).
97. Qian, H. F., Zhu, M. Z., Gayathri, C., Gil, R. R. & Jin, R. C. Chirality in gold nanoclusters probed by NMR spectroscopy. *ACS Nano* **5,** 8935–8942 (2011).
98. Dolamic, I., Knoppe, S., Dass, A. & Thomas Bürgi, T. Chiral gold nanoclusters protected by achiral ligands: first enantioseparation and circular dichroism spectra of $Au_{38}(SCH_2CH_2Ph)_{24}$. *Nature Commun.* **3,** 798 (2012).
99. Lopez-Acevedo, H., Tsunoyama, T., Tsukuda, H., Häkkinen, H. & Aikens, C. M. Chirality and electronic structure of the thiolate-protected Au_{38} nanocluster. *J. Am. Chem. Soc.* **132,** 8210–8218 (2010).
100. Aviram, A. & Ratner, M. A. Molecular rectifiers. *Chem. Phys. Lett.* **29,** 277–283 (1973).
101. Ratner, M. A. Introducing molecular electronics. *Mater. Today* **5,** 20–27 (February, 2002).
102. Nitzan, A. & Ratner, M. A. Electron transport in molecular wire junctions. *Science* **300,** 1384–1389 (2003).
103. Bumm, L. A. *et al.* Are single molecular wires conducting? *Science* **271,** 1705 (1996).
104. Agrait, N., Levy-Yeyati, A. & van Ruitenbeek, J. M. Quantum properties of atomic-scale conductors. *Phys. Rep*. **377,** 81–380 (2003).
105. Reed, M. A., Zhou, C., Muller, C. J., Burgin, T. P. & Tour, J. M. Conductance of a molecular junction. *Science* **278,** 252–254 (1997).
106. Xiao, X, Xu, B. & Tao, N. J. Measurement of single molecule conductance: Benzenedithiol and benzenedimethanethiol. *Nano Lett.* **4,** 267–271 (2004).
107. Tsutsui, M., Teramae, Y., Kurokawa, S. & Sakai, A. High-conductance states of single benzenedithiol molecules. *Appl. Phys. Lett.* **89,** 163111 (2006).
108. Ulrich, J. *et al.* Variability of conductance in molecular junctions. *J. Phys. Chem. B* **110,** 2462–2466 (2006).
109. Lörtscher, E., Weber, H. B. & Riel, H. Statistical approach to investigating transport through single molecules. *Phys. Rev. Lett*. **98,** 176807 (2007).
110. Martin, C. A., Ding, D., van der Zant, H. S. J. & van Ruitenbeek, J. M. Lithographic mechanical break junctions for single-molecule measurements in vacuum: possibilities and limitations. *New J. Phys*. **10,** 065008 (2008).
111. Haiss, W. *et al.* Variable contact gap single-molecule conductance determination for a series of conjugated molecular bridges. *J. Phys. Condens. Matter* **20,** 374119 (2008).
112. Horiguchi, K., Tsutsui, M., Kurokawa, S. & Sakai, A. Electron transmission characteristics of Au/1,4-benzenedithiol/Au junctions. *Nanotechnology* **20,** 0252041 (2009).
113. Song, H., *et al.* Observation of molecular orbital gating. *Nature* **462,** 1039–1043 (2009).
114. Kim, Y., Hellmuth, T. J., Burkle, M., Pauly, F. & Scheer, E. Characteristics of amine-ended and thiol-ended alkane single-molecule junctions revealed by inelastic electron tunnelling spectroscopy. *ACS Nano* **5,** 4104–4111 (2011).
115. Kim, Y., Pietsch, T., Erbe, A., Belzig, W. & Scheer, E. Benzenedithiol: a broad range single-channel molecular conductor. *Nano Lett*. **11,** 3734–3738 (2011).
116. Di Ventra M, Pantelides, S. T. & Lang, N. D. First-principles calculation of transport properties of a molecular wire. *Phys. Rev. Lett.* **84,** 979–982 (2000).
117. Basch, H., Cohen, R. & Ratner, M. A. Interface geometry and molecular junction conductance: Geometric fluctuation and stochastic switching. *Nano Lett*. **5,** 1668–1675 (2005).
118. Andrews, D. Q., Van Duyne, R. P. & Ratner, M. A. Stochastic modulation in molecular electronic transport junctions: molecular dynamics coupled with charge transport calculations. *Nano Lett*. **8,** 1120–1126 (2008).

119. Yeganeh, S., Ratner, M. A., Galperin, M. & Nitzan, A. Transport in state space: voltage-dependent conductance calculations of benzene-1,4-dithiol. *Nano Lett*. **9,** 1770–1774 (2009).
120. Solomon, G. C., Herrmann, C., Hansen, T., Mujica, V. & Ratner, M. A. Exploring local currents in molecular junctions. *Nature Chem*. **2,** 223–228 (2010).
121. Strange, M., Lopez-Acevedo, O. & Häkkinen, H. Oligomeric gold-thiolate units define the properties of the molecular junction between gold and benzene dithiols. *J. Phys. Chem. Lett.* **1,** 1528–1532 (2010).
122. Sergueev, N, Tsetseris, L., Varga, K. & Pantelides, S. Configuration and conductance evolution of benzene–dithiol molecular junctions under elongation. *Phys. Rev. B* **82,** 073106 (2010).
123. Reuter, M. G., Seideman, T. & Ratner, M. A. Guidelines for choosing molecular 'alligator clip' binding motifs in electron transport devices. *J. Chem. Phys*. **134,** 154708 (2011).
124. Pontes, R. B., Rocha, A. R., Sanvito, S., Fazzio, A. & da Silva, A. J. R. Ab initio calculations of structural evolution and conductance of benzene-1,4-dithiol on gold leads. *ACS Nano* **2,** 795–804 (2011).
125. Strange, M., Rostgaard, C., Häkkinen, H. & Thygesen, K. S. Self-consistent GW calculations of electronic transport in thiol- and amine-linked molecular junctions. *Phys. Rev. B* **83,** 115108 (2011).
126. Lopez-Acevedo, O., Kacprzak, K. A., Akola, J. & Häkkinen, H. Quantum size effects in ambient CO oxidation catalysed by ligand-protected gold clusters. *Nature Chem.* **2,** 329 (2010).
127. Vericat, C., Benitez, G. A., Grumelli, D. E., Vela, M. E. & Salvarezza, R. C. Thiol-capped gold: from planar to irregular surfaces. *J. Phys.: Condens. Matter* **20,** 184004 (2008).
128. Dass, A. Faradaurate nanomolecules: a superstable plasmonic 76.3 kDa cluster. *J. Am. Chem. Soc.* **133,** 19259–19261 (2011).
129. Qian, H., Zhu, Y. & Jin, R. C. Atomically precise gold nanocrystal molecules with surface plasmon resonance. *Proc. Natl Acad. Sci. USA* http://dx.doi.org/10.1073/pnas.1115307109 (2012).
130. Zhu, Z-J. *et al.* Stability of quantum dots in live cells. *Nature Chem*. **3,** 963–968 (2011).
131. Akola, J. *et al.* Materials from thiolate-protected Au_{25} superatoms: dimers and crystals. *J. Phys. Chem C* **114,** 15986 (2010).

Acknowledgements

I am indebted to collaborators and co-authors of refs. 35, 38, 56, 75, 77–82, 99, 121, 125, 126 and 131, and I thank C. J. Ackerson for useful comments on the manuscript. This work has long-standing support from the Academy of Finland and the CSC—the Finnish IT Center for Science.

Additional information

The author declares no competing financial interests. Reprints and permissions information is available online at http://www.nature.com/reprints. Correspondence should be addressed to H.H.